PCCP

PAPER

View Article Online
View Journal | View Issue

Cite this: *Phys. Chem. Chem. Phys.*, 2014, **16**, 12959

Diastereomeric preference of a triply axial chiral binaphthyl based molecule: a concentration dependent study by chiroptical spectroscopies†

Zahra Dezhahang,[a] Mohammad Reza Poopari,[a] Florencio Eloy Hernández,[b] Carlos Diaz[b] and Yunjie Xu*[a]

We have examined the effects of environmental perturbations, specifically solvents and concentrations, on axial chirality of a recently synthesized axially chiral binaphthyl fluorene based salen ligand, named AFX-155, {[2,2′-(1*E*,1′*E*)-(*R*)-1,1′-binaphthyl-2,2′-diylbis(azan-1-yl-1-ylidene)bis(methan-1-yl-1-ylidene)bis(4-((7-(diphenylamino)-9,9-dihexyl-9*H*-fluoren-2-l)ethynyl)-phenol)]}. Chirality and dominant conformations of AFX-155 in $CDCl_3$ solvent have been characterized using vibrational absorption (VA) and vibrational circular dichroism (VCD) spectroscopy in combination with DFT calculations. AFX-155 exhibits triple axial chirality: one is at the binaphthyl ring and the other two are related to the axes of chirality along the –C–N bonds where Cs are part of the binaphthyl group. To evaluate solvent and concentration dependence, complementary VA and VCD experiments in both THF-d_8 and $CDCl_3$ have been performed, as well as the optical rotatory dispersion (ORD) and electronic CD (ECD) measurements in $CDCl_3$ under much diluted conditions. While the binaphthyl chirality is determined by the synthetic route, the results show that the latter two axial chirality labels of the dominant diastereomers are concentration dependent. Under much diluted conditions, *R*-binaphthyl, *R_intra*_HB//*R_extra*_HB (*R-RR*) is favoured, whereas *R*-binaphthyl, *S_intra*_HB//*S_extra*_HB (*R-SS*) is the dominant species in a concentrated solution. This diastereomeric interconversion is found to be independent of the two solvents used. To provide insights into this interesting finding, conformational searches and the related spectral simulations have been carried out at the DFT/B3LYP/6-31G(d) level.

Received 19th April 2014,
Accepted 7th May 2014

DOI: 10.1039/c4cp01704h

www.rsc.org/pccp

1 Introduction

It is well known that solvent can exert a deciding influence on the preferred conformation and even chirality of a chiral solute in solution.[1,2] Such effects are often manifested in severe and sometimes non-intuitive effects on chiroptical spectral signatures. Both solvent polarity and hydrogen (H)-bonding formation between solute and solvent molecules can influence the chiroptical response.[3,4] For example, the experimental vibrational circular dichroism (VCD) spectra of methyl mandelate look quite different in chloroform, methanol, and dimethyl sulfoxide (DMSO). While the spectrum in chloroform can be well reproduced by the gas phase simulation, it is necessary to apply the explicit solvention model to account for the spectra in the other two solvents.[5] In another example, chiral poly(ureidophthalimide) foldamers were reported to adopt two opposite helical handedness in water and in tetrahydrofuran (THF) where mirror imaged electronic CD (ECD) bands were detected.[6] Such solvent effects allow one to control over the helical architecture and direct the supramolecular synthesis. Similarly, solvent-mediated chirality switching was reported for dendrimer folding in aqueous solution.[7] Generally speaking, polar protic solvents, such as water can disrupt intra- and intermolecular electrostatic and H-bonding interactions of the example systems discussed above thereby changing the relative stabilities of various conformational assemblies.[8]

Much less reported is the concentration induced conformational change in common organic solvents used for chiroptical spectroscopic studies, such as DMSO, deuterated chloroform ($CDCl_3$) or THF. This is an interesting and important topic since several commonly used chiroptical spectroscopic tools for absolute configuration and conformational determination of chiral compounds, such as VCD and ECD, Raman optical

[a] *Department of Chemistry, University of Alberta, Edmonton, Alberta, Canada T6G 2G2. E-mail: Yunjie.xu@ualberta.ca; Fax: +1-780-492-8231; Tel: +1-780-492-1244*
[b] *Department of Chemistry and CREOL/the College of Optics and Photonics, University of Central Florida, P.O. Box 162366, Orlando, Florida 32816-2366, USA. E-mail: Florencio.Hernandez@ucf.edu; Fax: +1-407-823-5222; Tel: +1-407-823-0843*

† Electronic supplementary information (ESI) available. See DOI: 10.1039/c4cp01704h

activity (ROA), and optical rotatory dispersion (ORD) spectroscopy, operate under very different concentration regimes and each has its own advantages and disadvantages. For example, VCD spectroscopy generally provides very rich band structures which often contain detailed structural information. Furthermore, VCD simulations are considerably more reliable than ECD and ORD since only ground electronic state calculations are needed.[9] On the other hand, an ECD or ORD experiment requires much less sample than VCD. While a typical concentration used for an ECD or ORD experiment is in the range of 10^{-5} to 10^{-3} M, the concentrations needed for VCD experiments are normally 10^{-1} to a few M and often saturated solution is used. In addition, each of these spectroscopy techniques probes only a certain molecular property. Consequently, a number of researchers have advocated using more than one of the spectroscopic monitoring tools in order to reach a reliable absolute configuration determination, providing there are no major structural changes with concentration.[10–13]

The susceptibility of axial chirality to the environmental perturbations such as the choice of different solvents and concentrations of the sample is the subject of significant practical and fundamental importance in supramolecular assembly.[14] We chose AFX-155, a triply axial chiral binaphthyl fluorene based salen ligand, *i.e.* [2,2′-(1*E*,1′*E*)-(*R*)-1,1′-binaphthyl-2,2′-diylbis(azan-1-yl-1-ylidene)bis(methan-1-yl-1-ylidene)bis(4-((7(diphenylamino)-9,9-dihexyl-9*H*-fluoren-2-l)ethynyl)-phenol)], as our targeted molecular system. AFX-155 is a model axial chiral system, with a good number of possible diastereomers and a few potential H-bonding sites. This molecule was recently synthesized for its potential applications in homogeneous catalysis, biophotonics, and biosensing.[15,16] It was also characterized using ECD and two-photon CD (TPCD) spectroscopy by Hernández and co-workers.[15,16]

One of our goals is to utilize VCD spectroscopy and DFT calculations to clearly establish the axial chirality of AFX-155 in solution. A second goal of our study is to examine the effects of environmental perturbations, *i.e.* solvent and concentrations, on axial chirality of AFX-155. To achieve that, we carried out VA and VCD experiments in THF and $CDCl_3$, as well as ORD and ECD measurements in $CDCl_3$ under much diluted conditions. From the combined experimental and theoretical results, we reached a surprising and interesting conclusion that the preferred axial chirality at the –C–N bonds is switched under concentrated and much diluted conditions. Further theoretical modeling was also performed to help to rationalize the observed phenomena.

2 Experimental and theoretical details

AFX-155 was synthesized using the reported Scheme 1 according to ref. 15 and 16. VA and VCD spectra were measured using a Bruker FTIR (Vertex 70) spectrometer equipped with a PMA 50 module for VCD measurements.[17] The data were collected at 4 cm^{-1} resolution in the wavenumber region of 1700–1100 cm^{-1} using a liquid nitrogen cooled MCT detector for a period of 4 hours (~4300 scans per an hour). 0.046 M solutions of AFX-155 in $CDCl_3$ and THF-d_8 were used for the VA and VCD measurements. The solution samples were placed between a pair of BaF_2 windows with a path-length of 0.125 mm.

For ORD measurements, a solution of 6.5×10^{-4} M AFX-155 in $CDCl_3$ was prepared using a 10 cm cell. The ORD data were collected at a series of wavelengths, namely at 589 nm of a sodium D line, and at 578 and 546 nm of a mercury lamp by means of a Perkin-Elmer 240 polarimeter. The solution with the same concentration is used to carry out the ECD data acquisitions. To meet spectroscopic criteria for CD measurements, the magnitude of the absorption is adjusted using a UV spectrometer and a 1 mm cell was used. An Olis DSM 17 CD spectrometer and a Hewlett Packard 8453 UV-VIS Spectrophotometer were used for ECD and UV measurements, respectively.

The Gaussian 09[18] program was used for all geometrical searches and optimizations, harmonic frequency calculations, and VA and VCD intensity predictions using density functional theory (DFT).[19] The well-known Becke three parameter, Lee–Yang–Parr, functional (B3LYP)[20] was used for the calculations. AFX-155 contains 224 atoms. This makes the usage of a high level of quantum chemical calculations prohibitively expensive. The 6-31G(d) basis set[21] was chosen since it offers a good combination of accuracy and computational efficiency. In an effort to better capture the relative stability of the potential conformers, single point energy calculations were also performed with the cc-pVTZ basis set.[22] In addition, we also carried out geometry optimizations for the targeted conformers with the D3 version of Grimme's dispersion method[23] using B3LYP/6-31G(d).

To account for the bulk solvent environment, the integral equation formalism (IEF) version of the polarizable continuum model (PCM) using the universal force field radii[24,25] was used. In a few previous studies, it was shown that the strength of H-bonding interaction between the chiral solute and $CDCl_3$ is not strong enough to demand an explicit treatment.[26,27] For this purpose, the dielectric constant of chloroform, $\varepsilon = 4.7113$, was used. A Lorentzian line shape with a half-width at half-height of 4 cm^{-1} was used for the simulations of VA and VCD spectra.

The time dependent density functional theory (TD-DFT) method with B3LYP/6-31G(d) was employed for all excited state energies, oscillator strength and optical rotation dispersion calculations. The first 80 electronic states were taken into account for theoretical ECD spectral simulations. To account for bulk of the solvent environment, the PCM model of chloroform was applied, as it was used for VA and VCD spectral simulations. For comparison to the experimental measurements, the half-width at half height (HWHH) of 0.2 eV with a Gaussian line-shaped function was used to simulate ECD spectra. We noted that in the previous work,[15] a broader Gaussian line-shaped function with 0.35 eV HWHH was used on the truncated systems where four $-C_6H_{13}$ groups were replaced by four methyl groups.[15]

3 Results and discussion

3.1 Possible diastereomers of AFX-155

Fig. 1 shows the chemical structure of this relatively large and flexible triply axial chiral molecule. AFX-155 possesses three

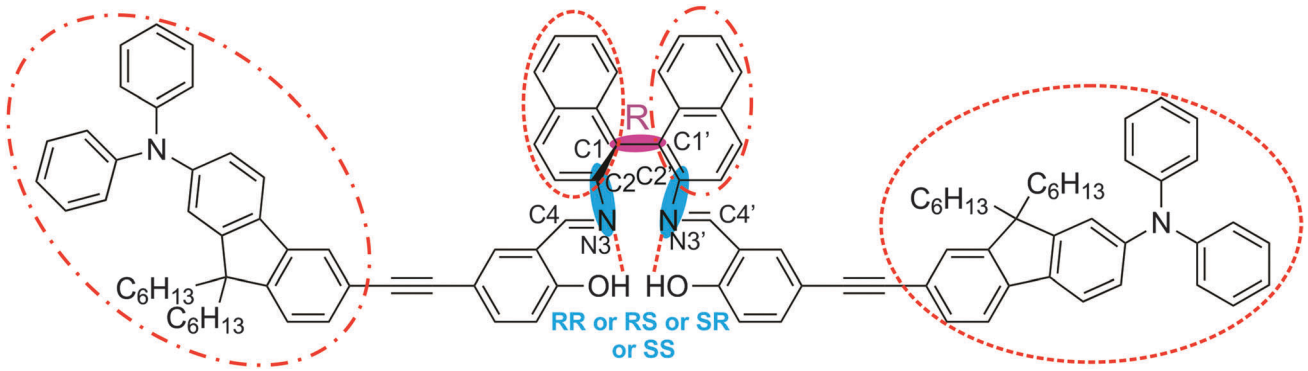

Fig. 1 Chemical structure of AFX-155 studied in this paper. There are three chiral axes: one at the binaphthyl ring and two along the C–N bonds. All of the chiral axes are highlighted with shades. Chirality of the binaphthyl ring is *R*, while the associated chirality at the –C–N bonds can be *RR*, *RS*, *SR* or *SS*. The two large substitutes about the –C═N bond take on the *trans*-arrangement shown here. The pair of the bulky group and the opposite binaphthyl half marked with dashed circles (or with dotted–dashed circles) can be in either extra or *intra* orientation (see Fig. S1 for further details, ESI†). In addition, the –OH···N═C intramolecular H-bonding interactions are indicated with dashed lines. See the text for further details.

chiral axes: one chiral axis for the binaphthyl ring and two others along the –C–N bonds where the carbon atoms are part of the binaphthyl group. The three chiral axes are highlighted in Fig. 1. In addition to the chirality labels, there are *cis*- and *trans*-conformations about the –C═N bond, *intra* and *extra* relative orientations of the salicylaldehyde moiety with respect to the other binaphthyl half, finally HB and NHB labels to indicate the existence or the non-existence of the –OH···N═C– intramolecular HB interaction, respectively. Based on the synthesis procedure of AFX-155, the chirality of the binaphthyl ring is determined to be *R*. For easy comparison with the previous publications on AFX-155, we have adopted the same axial chirality labels along the–C–N bonds as used in ref. 15. The details about the axial chirality and *intra* and *extra* labels are provided in Fig. S1, ESI.†

3.2 Experimental VCD spectra of AFX-155

VA and VCD spectra of the AFX-155 molecule in weakly polar deuterated chloroform, *i.e.* $CDCl_3$, are presented in Fig. 2. $CDCl_3$ was chosen as it offers sufficient solubility and does not interfere in the IR window from 1700–1100 cm^{-1}. Since the previous ECD study[15,16] was carried out in deuterated THF solvent, *i.e.* THF-d_8, we also perform further VA and VCD measurements in THF-d_8 for comparison. The resulting VA and VCD spectra in THF are also included in Fig. 2 for comparison. Generally, the raw VA spectra of AFX-155 in these two solvents, *i.e.* without solvent subtraction, look somewhat different because of different solvent bands. In the 1700–1200 cm^{-1} region, the VCD band features, on the other hand, look very much the same in both solvent, suggesting that the conformational landscape and the associated axial chirality of AFX-155 remain unchanged in these two solvents. Since $CDCl_3$ provides a wider VCD spectral window in the current study, for simplicity, we will use VA and VCD spectra in $CDCl_3$ for the spectral analyses in the remainder of this paper, unless indicated otherwise.

3.3 Comparison of experimental and simulated VCD spectra of AFX-155

A systematic conformational search for AFX-155 was reported in ref. 15. All *cis*-conformers were found to be substantially less stable than *trans*-conformers due to severe steric effects in the former case. Therefore only *trans*-conformers are considered here. For simplicity, we drop the prefix *trans* for all conformers in the current study. We would also like to point out that in the

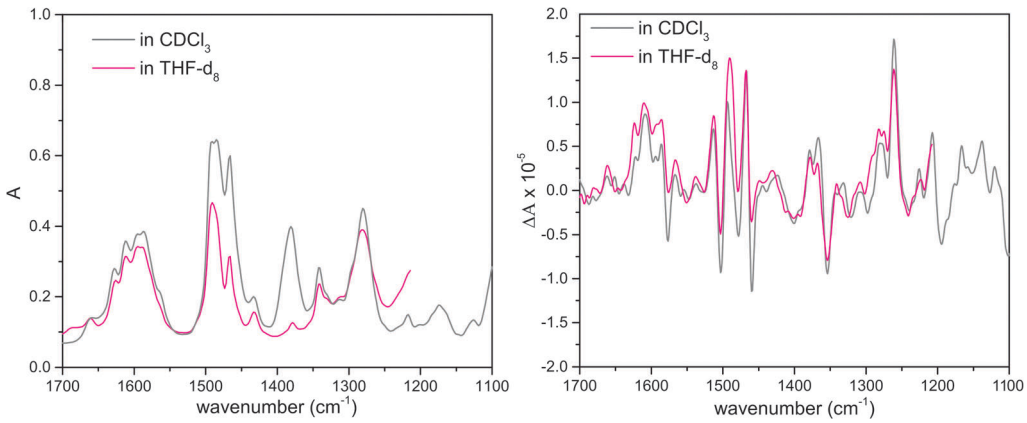

Fig. 2 Raw experimental VA (left) and VCD (right) spectra of AFX-155 in deuterated chloroform and THF-d_8 solvents. The measurements below 1200 cm^{-1} in THF are removed due to strong THF solvent absorption.

previous study, the four alkyl chains ($-C_6H_{13}$) were replaced by four $-CH_3$ subunits to reduce computational cost because it was rationalized that these chains do not have any significant contributions to the electronic transitions. Since VCD spectral features are much more sensitive to subtle conformational changes, we decide to include these alkyl chains in our geometry optimizations and VA and VCD spectral simulations.

One noticeable outcome with the inclusion of the four alkyl chains is that the number of possible conformers is reduced because of the additional steric hindrance introduced by these bulky subunits. In total nine HB conformers are re-optimized and are confirmed to be real minima. Their geometries are presented in Fig. 3 where we separate these structures obtained into three groups, based on their associated axial chirality at the –C–N bonds, *i.e. RR*, *RS*, or *SS*. It is interesting to note that the long bulky side chains form cavities of different sizes in different conformers. As a result, one may anticipate that accessibility to solvent molecules can vary quite differently among various conformers. For example, the *R_intra*_HB//*S_extra*_HB conformer is structurally fully extended whereas *R_extra*_HB//*R_extra*_HB is considerably more compact, with a much smaller cavity size (see Fig. S2, ESI†).

The relative energies and free energies of these three groups of conformers using B3LYP/6-31G(d), single point energy at B3LYP/cc-pVTZ//6-31G(d) and using B3LYP/6-31G(d) with the D3 Grimme's dispersion correction are summarized in Table S1, ESI.† We note that the inclusion of the dispersion interactions can change the relative energies significantly. For example, *S_extra*_HB//*S_extra*_HB is more stable than *S_intra*_HB//*S_extra*_HB and *S_intra*_HB//*S_intra*_HB by a few kcal mol^{-1} without the inclusion of dispersion interactions. With the inclusion of dispersion interactions, *S_intra*_HB//*S_extra*_HB becomes the most stable one by more than 15 kcal mol^{-1} compared to the other two. It is no surprise that dispersion energy becomes important for systems like AFX-155, but we also stress the considerable current challenges in obtaining reliable relative energies for a large system like AFX-155 in general.

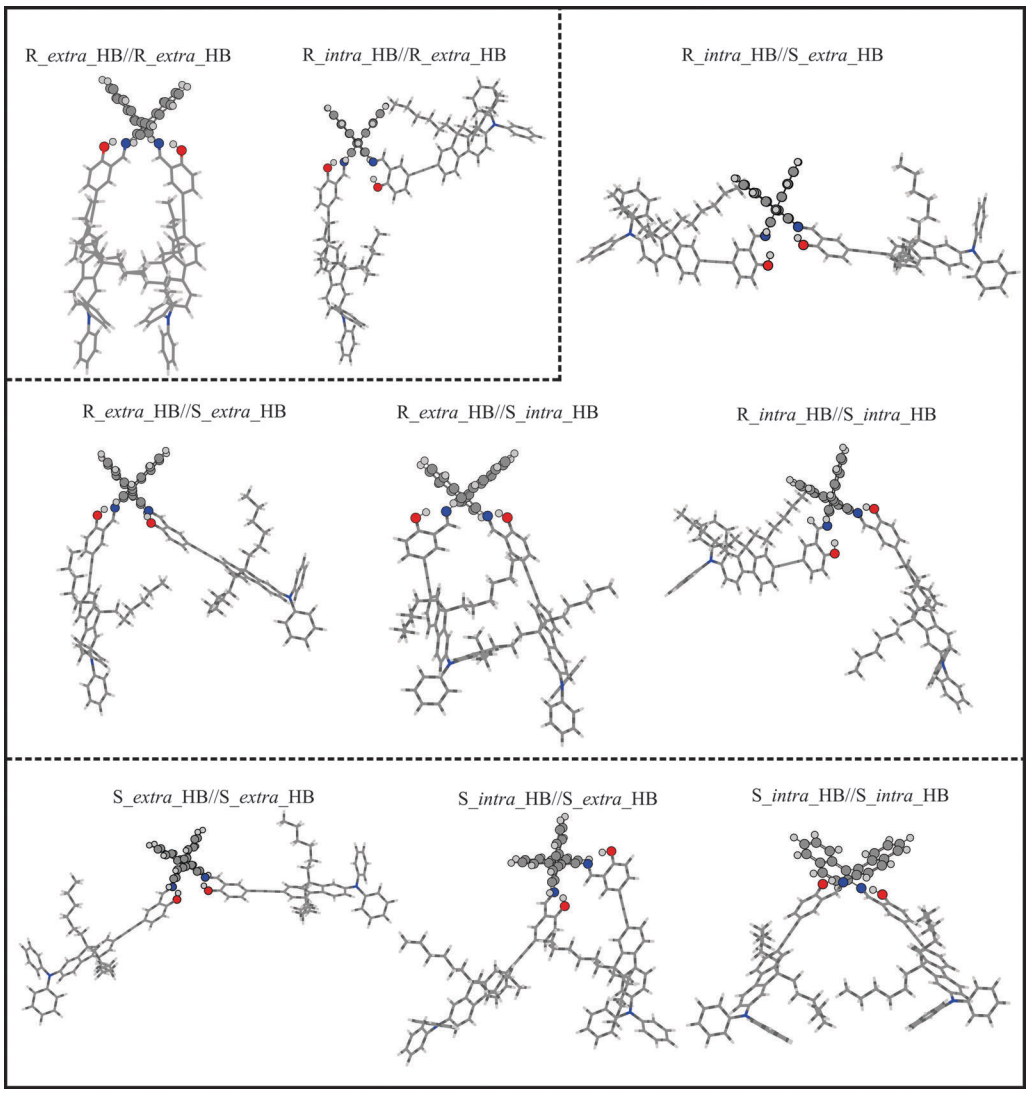

Fig. 3 Optimized geometries of the HB conformers of AFX-155 in $CDCl_3$ obtained at the PCM/B3LYP/6-31G(d) level of theory. The geometries are separated into three groups based on their associated axial chirality at the –C–N bonds, *i.e. RR*, *RS*, or *SS*.

In addition to the HB conformers, the relevant HB//NHB and NHB conformers are also considered and their geometries re-optimized. We note that those conformers with two intramolecular HB bonds are considerably more stable than those with one and even more so than those without in each of the three groups indicated above. This is consistent with other previous studies that suggest that species with the intramolecular H-bonding interactions become dominant over those without in the presence of non-polar or weakly polar solvent such as CH_2Cl_2 and $CHCl_3$.[28]

In Fig. 4, we compare the calculated VA and VCD spectra of all HB conformers of AFX-155. Since AFX-155 is fairly large and has a significant number of vibrational modes in the finger print region, many of these VA bands overlap with each other. This often makes direct and detailed comparison between experimental and theoretical VA spectra ambiguous and prevents one to draw decisive structural information. On the other hand, VCD spectra tend to show a considerable amount of unique spectral signatures related to stereogenic and conformational structural information. For comparison between theory and experiment, we divide the finger print region into three sections from high to low wavenumbers and refer to Fig. 1 for the functional groups indicated below. Region I from 1700 to 1550 cm^{-1} is composed of several strong vibration bands due to the C=N stretching, O–H bending, and C=C stretching of the binaphthyl rings. Region II from 1550 to 1400 cm^{-1} contains mostly vibrational motions associated with the C–H and O–H bending of the two phenyl groups which are in close proximity to the binaphthyl rings, the C–H bending of the aromatic rings of the two bulky end substitutes, and the CH_2 scissoring of the four C_6H_{13} alkyl chains. Region III from 1400–1100 cm^{-1} contains mainly C–N stretching at the two bulky terminal groups and CH_2 bending of the long alkyl chain. Overall, the simulated IR spectra of all nine HB conformers presented in Fig. 4 look all alike. Furthermore, they all agree well with the experimental VA data. Therefore, one cannot differentiate these conformers on the basis of their VA spectral signatures.

The theoretical VCD spectral features, on the other hand, look substantially different from one conformer to the next,

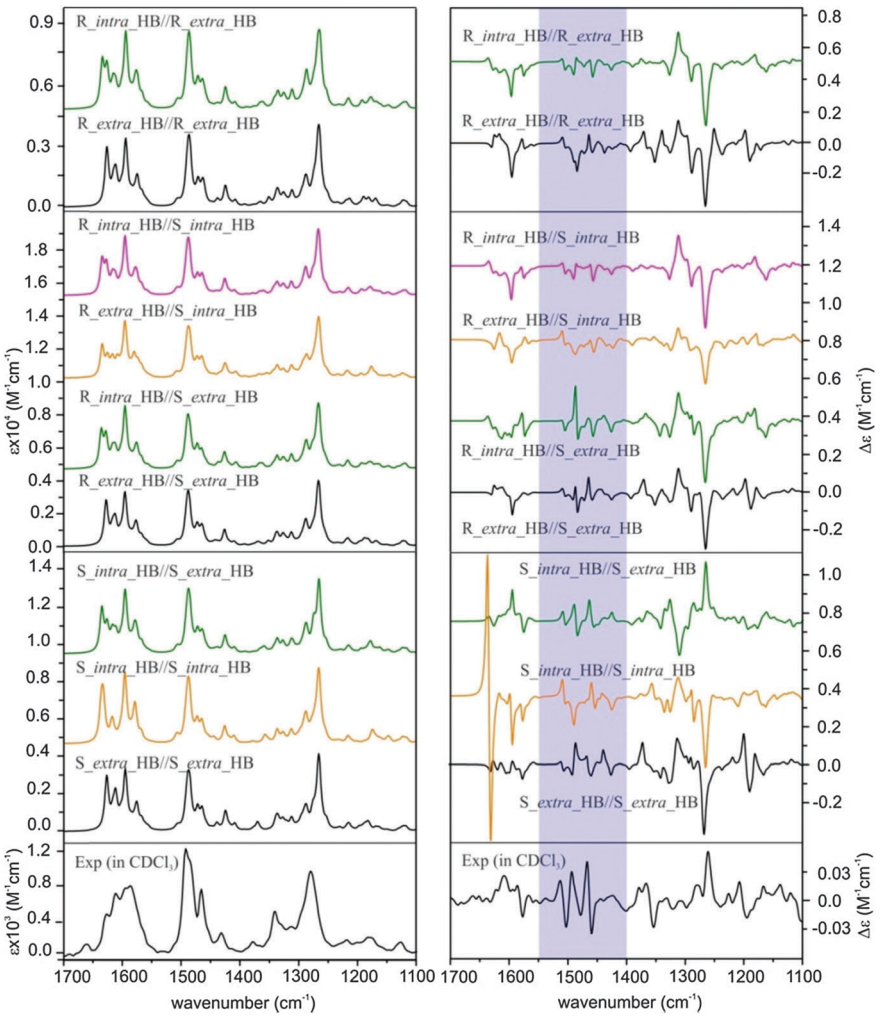

Fig. 4 Calculated VA (left) and VCD (right) spectra of all nine HB conformers of AFX-155 obtained at the PCM/B3LYP/6-31G(d) level compared to the experimental data at the bottom. For easy comparison, these conformers are separated into three groups based on the associated axial chirality at the –C–N bonds, *i.e. RR*, *RS*, or *SS*.

enabling potentially clear identification of the dominant conformational species in solution. This highlights the significant advantages of VCD spectroscopy in providing structural information of chiral systems in solution. Below, we compare the simulated VCD features of each HB conformers among themselves and with the major experimental VCD spectral features in all three finger print regions. In region I, the prominent experimental positive and negative VCD band at 1610 cm^{-1} and 1577 cm^{-1}, respectively, can only be matched by conformers *R_extra*_HB//*S_extra*_HB and *S_intra*_HB//*S_extra*_HB while all the other conformers exhibit major discrepancy. Although the smaller experimental VCD features in this region are somewhat noisy, the consistency they show in both $CDCl_3$ and THF-d_8 solvents gives one confidence in their reliability. In region II (shaded), the experimental VCD spectrum shows a beautiful sequence of +/−/+/−/+/− VCD signatures. This sequence is best matched with *S_intra*_HB//*S_extra*_HB, while all the other conformers exhibit markedly different patterns with the exception of perhaps *R_intra*_HB//*S_extra*_HB. The latter one demonstrates a somewhat similar pattern but with an additional negative band at the high wavenumber end. In region III, the most prominent experimental VCD feature at ~1270 cm^{-1} is positive, while a negative band is predicted for all HB conformers except *S_intra*_HB//*S_extra*_HB, which exhibits a positive VCD band feature. From the above detailed comparison, it is clear that *S_intra*_HB//*S_extra*_HB is the only HB conformer which demonstrates consistent agreement with the experimental data in all three regions.

Since the previous ECD study indicated that the *R_intra*_NHB//*R_extra*_NHB conformer provides the best agreement between simulated and experimental ECD spectra, we also compare simulated VA and VCD spectra of all the relevant *R_intra*//*R_extra* HB and NHB conformers and *S_intra*//*S_extra* HB and NHB conformers in Fig. 5 for completion.

From Fig. 5, it is immediately obvious that all *R_intra*//*R_extra* HB or NHB conformers show major discrepancies in the VCD features in the 1300–1200 cm^{-1} region. For the *S_intra*//*S_extra* conformers, the agreements between experiment and theory seem to be generally better than *R_intra*//*R_extra* at the first glance. Detailed comparison of VA and VCD

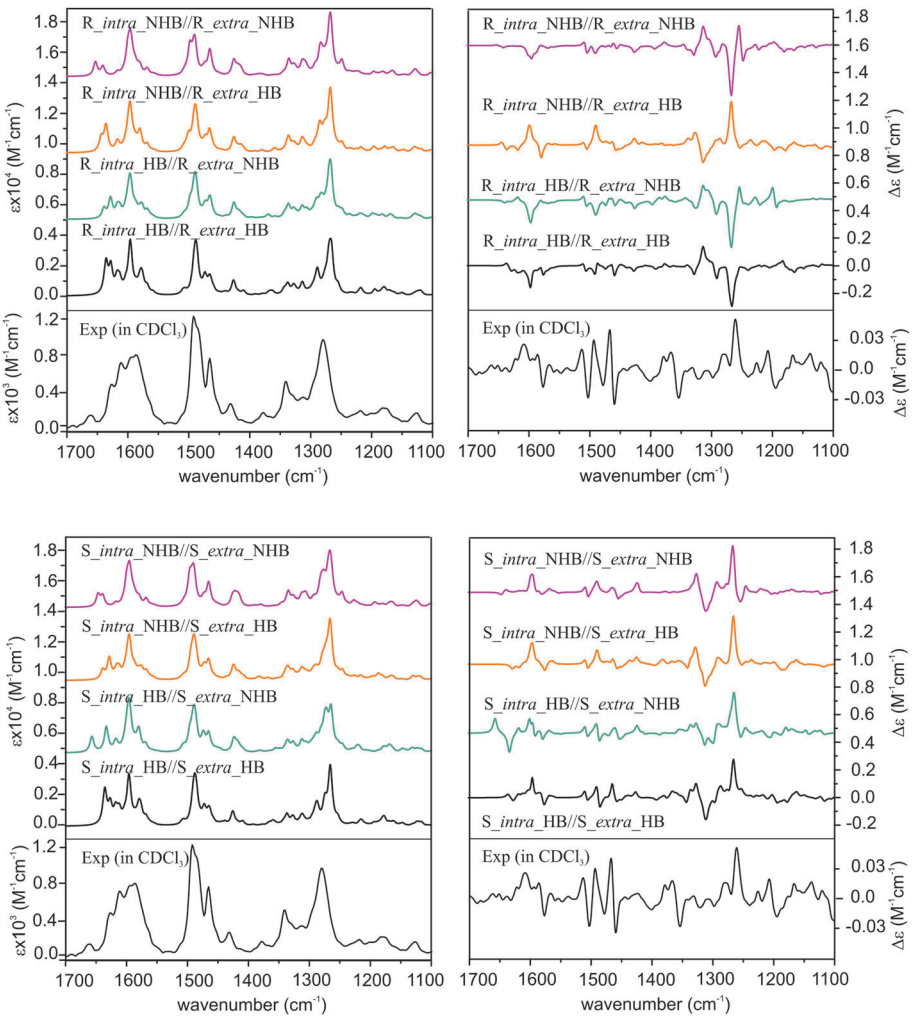

Fig. 5 Calculated VA (left) and VCD (right) spectra of all the *R_intra*//*R_extra* HB or NHB conformers (top panel) and *S_intra*//*S_extra* HB or NHB conformers (bottom panel) of the AFX-155 molecule obtained at the PCM/B3LYP/6-31G(d) level compared with the experimental ones.

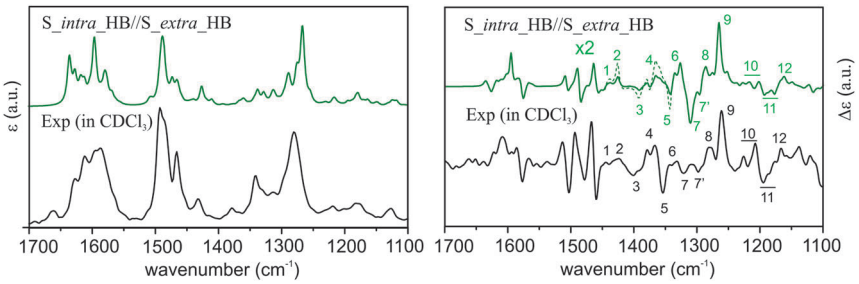

Fig. 6 Comparison of the experimental VA and VCD spectra of AFX-155 in $CDCl_3$ with the corresponding simulated spectra of *S_intra*_HB_*S_extra*_HB obtained at the PCM/B3LYP/6-31G(d) level of theory. The theoretical VCD band intensities in a small region between 1450 cm^{-1} and 1330 cm^{-1} are amplified by a factor of 2 and indicated with a dotted line for easier pattern recognition. The Arabic numerals are used to indicate the corresponding features in the experimental and theoretical data in the crowded region below 1450 cm^{-1}.

spectra of *S_intra*_HB//*S_extra*_HB with the experimental data is summarized in Fig. 6. While the existence of other *S_intra*//*S_extra* NHB conformers in small amounts cannot be ruled out completely, *S_intra*_HB//*S_extra*_HB is evidently by far the dominant species. This preference for the HB species observed here is also consistent with the discussion on the relative energies above.

3.4 Concentration dependent diastereomeric preference

Based on the distinctive VCD spectral features described above, we can conclusively identify *S_intra*_HB//*S_extra*_HB as the dominant species in $CDCl_3$. This conclusion, however, is in odd with the previous ECD and TPCD investigations of AFX-155 where *R_intra*//*R_intra* diastereomers were identified as the main species. This prompts us to ask a few interesting and important questions. Why do the previous ECD and the present VCD studies come to such different conclusions? Are there really different dominant species in $CDCl_3$ in the present study and in THF-d_8 in the previous studies? If yes, what are the plausible explanations for such strong preference of different diastereomers in solution?

First, we examine if two different solvents, *i.e.* $CDCl_3$ and THF-d_8, are the cause for such noticeably different conclusions. For that, we already did the VA and VCD measurements in both solvents (see discussion before) and found no obvious difference in the VA and VCD spectral features of AFX-155 excluding absorption due to solvents themselves. Furthermore, both solvents have similar dielectric constants, 4.7113 and 7.4257, respectively. For completion, we also measured UV-Vis and ECD spectra in $CDCl_3$ (Fig. 7). As one can see, these spectra are very much the same as those obtained in the previous study using THF-d_8.[15] Therefore, solvents themselves seem not to be the main issue here.

Another noticeable difference is the concentrations used in ECD and VCD experiments. While ECD experiments typically use a highly diluted sample ($\leq 1 \times 10^{-3}$ M), a highly concentrated sample is needed for VCD measurements because VCD intensity is usually only 10^{-4} to 10^{-5} of VA bands. In the current experiment, a 70 fold higher concentration is used for VCD than ECD. For a more systematic comparison, we included also ORD measurements in $CDCl_3$. Furthermore, we performed both ECD and ORD simulations for all conformers of interest using their full geometries, in contrast to the previous ECD study

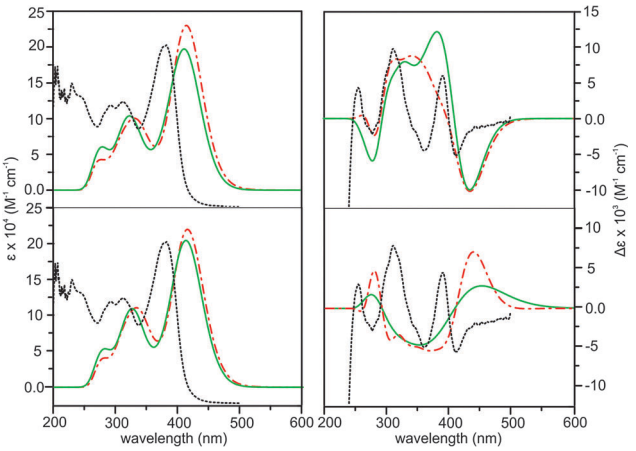

Fig. 7 Comparison of the experimental ECD spectrum in $CDCl_3$ (black dotted line) with the theoretical ECD spectra of *R_intra*//*R_extra* (upper row) and *S_intra*//*S_extra* (lower row) HB (red dashed–dotted line) and NHB (green solid line) conformers obtained at the PCM/B3LYP/6-31G(d) level of theory.

where some bulky groups $-C_6H_{13}$ were simplified with $-CH_3$ groups. The results are summarized in Fig. 7 and 8 for ECD and ORD spectra, respectively. Generally, the simulated ECD spectra are similar to those reported before, suggesting that the truncation used before is justified. While the agreement between ECD experimental and simulated spectra is not as decisive as the corresponding VCD counterparts, it is nevertheless quite clear here that the ECD features of *R_intra*//*R_extra* conformers are in accord with the observed data while *S_intra*//*S_extra* conformers show severe discrepancies. The experimental ORD spectrum shows an upward trend going from short to long wavelengths. While *R_intra*_HB//*R_extra*_HB exhibits the same upward trend in agreement with the experimental observation, *S_intra*_HB//*S_extra*_HB shows a downward trend. It is noted that although the absolute ORD values are still challenging to be reproduced theoretically, the general variation trend with wavelength is typically better reproduced.[29–31] Therefore the ORD study performed here also qualitatively supports the conclusion derived from both the current and previously reported ECD studies[15,16] that *R_intra*//*R_extra* is the dominant species in the much diluted solution, rather than *S_intra*//*S_extra*.

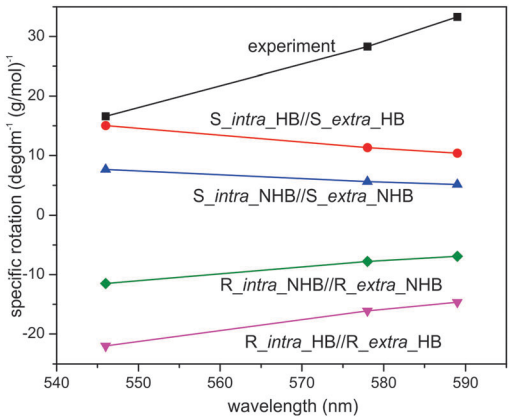

Fig. 8 Comparison of the experimental ORD spectrum in $CDCl_3$ with the theoretical ORD spectra of *R_intra*//*R_extra* HB and NHB conformers as well as *S_intra*//*S_extra* HB and NHB conformers obtained at the PCM/B3LYP/6-31G(d) level of theory.

It therefore appears that concentration plays a crucial role in which diastereomer is preferred in solution. Although such observations appear not to have been extensively studied, there are a number of theoretical and experimental publications when similar concentration dependent conformational preferences were reported.[32–34] For example, inversion of population distribution of felodipine conformations at increasing concentration in DMSO was observed by Khodov and co-workers in 2014.[33] Using NMR spectroscopy, these authors concluded that conformational preference of felodipine in DMSO is concentration dependent: conformers that dominate in a dilute solution become the least abundant in the saturated one. Furthermore, they pointed out that conformers that dominate in the saturated solution are of the same type as revealed in the crystalline state by X-ray. The authors attribute the inversion of conformer distribution in the saturated solution to both increases in intermolecular felodipine–felodipine and felodipine–DMSO interactions. Ghorai applied molecular dynamics simulations to predict the concentration dependence of *trans* and *gauche* conformations of *n*-butane inside a confined medium such as zeolite NaY.[34] He found that the percentage of *gauche* conformations inside zeolite increases with concentration and identified guest–guest interaction as the key factor for the enhancement of the *gauche* conformation.

To understand the observation, we performed a one-dimensional potential energy surface scan for the inter-conversion between *R_intra*_HB//*R_extra*_HB and *S_intra*_HB//*S_extra*_HB and found that the interconversion can occur through a planar TS with a barrier energy of 1.8 kcal mol^{-1} obtained at the B3LYP/3-21G level of theory. The interconversion between *R_intra*//*R_extra* and *S_intra*//*S_extra* conformers of AFX-155 is likely facilitated by solvent molecules. As indicated before, while *R_intra*//*R_extra* conformers exhibit a larger cavity, allowing easy access by solvent molecules, *S_intra*//*S_extra* conformers show a much smaller cavity (see Fig. S2, ESI†). One may expect that such differences in solvent–solute interactions may lead to preferentially stabilization of certain conformers, as recently reported in the case of a tris(diamine)nickel(II) complex.[35] Further theoretical modelling will be required to understand this interesting and important phenomenon in greater details, but that is out-of-scope of the current study.

Conclusions

Axial chirality and conformations of a flexible multiple axial chiral molecule, AFX-155, have been extensively investigated using three chiroptical spectroscopies, *i.e.* VCD, ECD, and ORD, in conjugation with DFT calculations. Experimentally, both VCD and ECD spectra of AFX-155 in THF-d_8 and $CDCl_3$ look essentially the same, indicating that the polarity of solvent does not influence the axial chirality and conformational distribution of AFX-155 significantly. The combined VCD and DFT study clearly shows that the dominant species is *R*-binaphthyl, *S_intra*_HB//*S_extra*_HB (*R-SS*) in the concentrated solution. In the much dilute solution, the dominant species is determined to be *R*-binaphthyl, *R_intra*_HB//*R_extra*_HB (*R-RR*) based on the ECD and ORD investigations. The latter conclusion is consistent with the previously reported ECD study. This is an area of research which has not yet been fully explored, although some theoretical and experimental publications had reported similar concentration dependent behaviors. Further theoretical modeling will be highly desirable to explain the interesting observations reported here in detail.

Acknowledgements

This research was funded by the University of Alberta and the Natural Sciences and Engineering Research Council of Canada. This research was enabled in part by support provided by WestGrid (www.westgrid.ca) and Compute Canada Calcul Canada (www.computecanada.ca). We gratefully acknowledge access to the computing facilities provided by the Shared Hierarchical Academic Research Computing Network (Sharcnet). The authors thank Dr Frazer for kindly providing the AFX-155 sample. YX holds a senior Canada Research Chair in Chirality and Chirality Recognition.

References

1 (*a*) B. Mennucci, C. Cappelli, R. Cammi and J. Tomasi, *Chirality*, 2011, **23**, 717–729; (*b*) P. Mukhopadhyay, G. Zuber, M. Goldsmith, P. Wipf and D. N. Beratan, *ChemPhysChem*, 2006, **7**, 2483–2486; (*c*) S. Coriani, A. Baranowska, L. Ferrighi, C. Forzato, D. Marchesan, P. Nitti, G. Pitacco, A. Rizzo and K. Ruud, *Chirality*, 2006, **18**, 357–369.

2 G. Yang and Y. Xu, in *Top. Curr. Chem.*, ed. R. Naaman, D. N. Beratan and D. H. Waldeck, Springer-Verlag, Berlin Heidelberg, 2011, vol. 298, pp. 189–236.

3 (*a*) P. L. Polavarapu, *Chirality*, 2012, **24**, 909–920; (*b*) M. R. Poopari, Z. Dezhahang, G. Yang and Y. Xu, *ChemPhysChem*, 2012, **13**, 2310–2321; (*c*) M. R. Poopari, P. Zhu, Z. Dezhahang and Y. Xu, *J. Chem. Phys.*, 2012,

137, 194308; (*d*) P. Zhu, G. Yang, M. R. Poopari, Z. Bie and Y. Xu, *ChemPhysChem*, 2012, **13**, 1272–1281.

4 Z. Dezhahang, M. R. Poopari and Y. Xu, *Chem. – Asian J.*, 2013, **8**, 1205–1212; C. Merten and Y. Xu, *Angew. Chem.*, 2013, **125**, 2127–2130 (*Angew. Chem., Int. Ed.*, 2013, **52**, 2073–2076).

5 M. R. Poopari, Z. Dezhahang and Y. Xu, *Phys. Chem. Chem. Phys.*, 2013, **15**, 1655–1665.

6 R. W. Sinkeldam, M. H. C. J. van Houtem, K. Pieterse, J. A. J. M. Vekemans and E. W. Meijer, *Chem. – Eur. J.*, 2006, **12**, 6129–6137.

7 A. L. Hofacker and J. R. Parquette, *Angew. Chem.*, 2005, **117**, 1077–1081 (*Angew. Chem., Int. Ed.*, 2005, **44**, 1053–1057).

8 (*a*) M. Losada, P. Nguyen and Y. Xu, *J. Phys. Chem. A*, 2008, **112**, 5621–5627; (*b*) M. Losada, H. Tran and Y. Xu, *J. Chem. Phys.*, 2008, **128**, 014508.

9 (*a*) T. Taniguchi and K. Monde, *J. Am. Chem. Soc.*, 2012, **134**, 3695–3698; (*b*) V. Andrushchenko, D. Tsankov, M. Krasteva, H. Wieser and P. Bour, *J. Am. Chem. Soc.*, 2011, **133**, 15055–15064; (*c*) T. Brotin, D. Cavagnat, J. Dutasta and T. Buffeteau, *J. Am. Chem. Soc.*, 2006, **128**, 5533–5540.

10 S. Abbate, F. Lebon, G. Longhi, C. F. Morelli, D. Ubiali and G. Speranza, *RSC Adv.*, 2012, **2**, 10200–10208.

11 P. Scafato, F. Caprioli, L. Pisani, D. Padula, F. Santoro, G. Mazzeo, S. Abbate, F. Lebon and G. Longhi, *Tetrahedron*, 2013, **69**, 10752–10762.

12 S. Qiu, E. De Gussem, K. Abbaspour Tehran, S. Sergeyev, P. Bultinck and W. Herrebout, *J. Med. Chem.*, 2013, **56**(21), 8903–8914.

13 L. Andernach, L. P. Sandjo, J. C. Liermann, I. Buckel, E. Thines and T. Opatz, *Eur. J. Org. Chem.*, 2013, 5946–5951.

14 P. L. Polavarapu, N. Jeirath, T. Kurtan, G. Pescitelli and K. Krohn, *Chirality*, 2009, **21**, E202–E207.

15 C. Diaz, A. Fraser, A. Morales, K. D. Belfield, S. Ray and F. E. Hernández, *J. Phys. Chem. A*, 2012, **116**, 2453–2465.

16 C. Díaz, L. Echevarria and F. E. Hernández, *J. Phys. Chem. A*, 2013, **117**, 8416–8426.

17 M. Losada and Y. Xu, *Phys. Chem. Chem. Phys.*, 2007, **9**, 3127–3135.

18 M. J. Frisch, G. W. Trucks, H. B. Schlegel, G. E. Scuseria, M. A. Robb, J. R. Cheeseman, G. Scalmani, V. Barone, B. Mennucci, G. A. Petersson, H. Nakatsuji, M. Caricato, X. Li, H. P. Hratchian, A. F. Izmaylov, J. Bloino, G. Zheng, J. L. Sonnenberg, M. Hada, M. Ehara, K. Toyota, R. Fukuda, J. Hasegawa, M. Ishida, T. Nakajima, Y. Honda, O. Kitao, H. Nakai, T. Vreven, J. A. Montgomery Jr., J. E. Peralta, F. Ogliaro, M. Bearpark, J. J. Heyd, E. Brothers, K. N. Kudin, V. N. Staroverov, R. Kobayashi, J. Normand, K. Raghavachari, A. Rendell, J. C. Burant, S. S. Iyengar, J. Tomasi, M. Cossi, N. Rega, J. M. Millam, M. Klene, J. E. Knox, J. B. Cross, V. Bakken, C. Adamo, J. Jaramillo, R. Gomperts, R. E. Stratmann, O. Yazyev, A. J. Austin, R. Cammi, C. Pomelli, J. W. Ochterski, R. L. Martin, K. Morokuma, V. G. Zakrzewski, G. A. Voth, P. Salvador, J. J. Dannenberg, S. Dapprich, A. D. Daniels, Ö. Farkas, J. B. Foresman, J. V. Ortiz, J. Cioslowski and D. J. Fox, *Gaussian 09, Revision D.01*, Gaussian, Inc., Wallingford CT, 2009.

19 (*a*) P. Hohenberg and W. Kohn, *Phys. Rev.*, 1964, **136**, B864–B871; (*b*) W. Kohn and L. J. Sham, *Phys. Rev.*, 1965, **140**, A1133–A1138; (*c*) J. K. Labanowski and J. W. Andzelm, *Density Functional Methods in Chemistry*, Springer-Verlag, New York, 1991.

20 (*a*) A. D. Becke, *J. Chem. Phys.*, 1993, **98**, 5648; (*b*) A. D. Becke, *Phys. Rev. A: At., Mol., Opt. Phys.*, 1988, **38**, 3098–3100; (*c*) T. Lee, W. T. Yang and R. G. Parr, *Phys. Rev. B: Condens. Matter Mater. Phys.*, 1988, **37**, 785–789.

21 P. C. Hariharan and J. A. Pople, *Theor. Chem. Acc.*, 1973, **28**, 213–222.

22 R. A. Kendall, T. H. Dunning Jr. and R. J. Harrison, *J. Chem. Phys.*, 1992, **96**, 6796–6806.

23 S. Grimme, J. Antony, S. Ehrlich and H. Krieg, *J. Chem. Phys.*, 2010, **132**, 154104.

24 J. Tomasi, B. Mennucci and R. Cammi, *Chem. Rev.*, 2005, **105**, 2999–3093.

25 B. Mennucci, J. Tomasi, R. Cammi, J. R. Cheeseman, M. J. Frisch, F. J. Devlin, S. Gabriel and P. J. Stephens, *J. Phys. Chem. A*, 2002, **106**, 6102–6113.

26 M. R. Poopari, Z. Dezhahang and Y. Xu, *Phys. Chem. Chem. Phys.*, 2013, **15**, 1655–1665.

27 Z. Dezhahang, C. Merten, M. R. Poopari and Y. Xu, *Dalton Trans.*, 2012, **41**(35), 10817–10824.

28 V. P. Nicu, E. J. Baerends and P. L. Polavarapu, *J. Phys. Chem. A*, 2012, **116**, 8366–8373.

29 P. Lahiri, K. B. Wiberg, P. H. Vaccaro, M. Caricato and T. D. Crawford, *Angew. Chem.*, 2014, **126**, 1410–1413 (*Angew. Chem., Int. Ed.*, 2014, **53**, 1386–1389).

30 P. Mukhopadhyay, G. Zuber, M. Goldsmith, P. Wipf and D. N. Beratan, *ChemPhysChem*, 2006, **7**, 2483–2486.

31 K. Ruud and R. Zanasi, *Angew. Chem.*, 2005, **117**, 3660–3662 (*Angew. Chem., Int. Ed.*, 2005, **44**, 3594–3596).

32 R. Begum, T. Sagawa, S. Masatoki and H. Matsuura, *J. Mol. Struct.*, 1988, **442**, 243–250.

33 I. A. Khodov, S. V. Efimov, M. Y. Nikiforov, V. V. Klochkov and N. Georgi, *J. Pharm. Sci.*, 2014, **103**, 392–394, DOI: 10.1002/JPS.23833.

34 P. Kr. Ghorai, *J. Phys. Chem. B*, 2010, **114**, 6492–6499.

35 C. Merten, R. McDonald and Y. Xu, *Inorg. Chem.*, 2014, **53**, 3177–3182.